Table S1. WTA fragments and theoretical *m/z* of their deprotonated pseudomolecular ions $[M-H]^-$

Name	$[M-H]^-$ (*m/z*)
Ribitol	151.06
GlcNAc	220.08
GlcNAc-Ribitol	354.14
Glc-GlcNAc-Ribitol	516.19
Gal-Glc-GlcNAc-Ribitol	678.25
GlcNAc-Ribitol Acetylated	396.15
Gal-GlcNAc-Ribitol Acetylated	558.20
Gal-Glc-GlcNAc-Ribitol Acetylated	720.26
GlcNAc-Ribitol-Phosphate	434.10
Glc-GlcNAc-Ribitol-Phosphate	596.15
Gal-Glc-GlcNAc-Ribitol-Phosphate	758.21
GlcNAc-GlcNAc-Ribitol	557.22
GlcNAc-GlcNAc-Ribitol Acetylated	599.22
Gal/Glc-GlcNAc-GlcNAc-Ribitol	719.27
GlcNAc-GlcNAc-GlcNAc-Ribitol	760.30
Rha-Ribitol	297.12
GlcNAc-Rha-Ribitol	500.20
Rha-Ribitol-Acetylated	339.13
GlcNAc-Rha-Ribitol Acetylated	542.21
Ala-Ribitol*	222.10
Glc-Ribitol	313.11
Ala-Glc-Ribitol*	384.15
Glc-Glc-Ribitol	475.17
Ala-Ribitol Acetylated*	264.11
Glc-Ribitol Acetylated	355.13
Ala-Glc-Ribitol Acetylated	426.16
Glc-Glc-Ribitol Acetylated	517.18
GlcNAc-Ribitol-Phosphate Acetylated	476.12
Glc-GlcNAc-Ribitol-Phosphate Acetylated	638.17
Gal-Glc-GlcNAc-Ribitol-Phosphate Acetylated	800.22
GlcNAc-Glycerol	294.12
Glc-GlcNAc-Glycerol	456.18
Glc-Glycerol	253.09
Glc-Glc-Glycerol	415.15
Glc-Glycerol Acetylated	295.10
GlcNAc Acetylated	262.09

* Species with alanine (Ala) not observed in *Listeria* WTA samples.

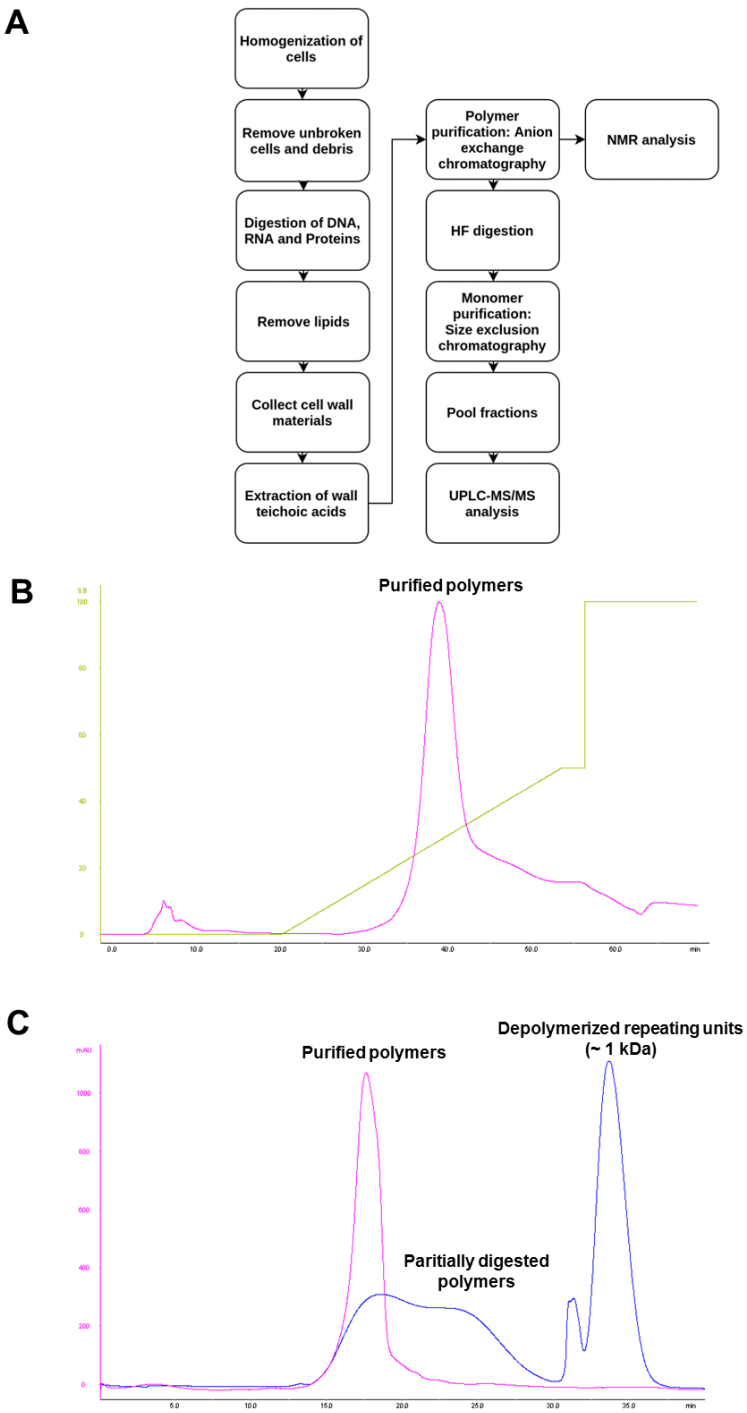

Figure S1. Extraction and purification of *Listeria* WTA polymers and depolymerized repeating units. (A) Experimental workflow of WTA purification and analysis by a combination of liquid chromatography, mass spectrometry and NMR spectroscopy. (B) Purification of polymers by anionic exchange chromatography with detection at 205 nm (mAu). (B) Purification of depolymerized repeating units by size-exclusion chromatography with detection at 205 nm (mAu).

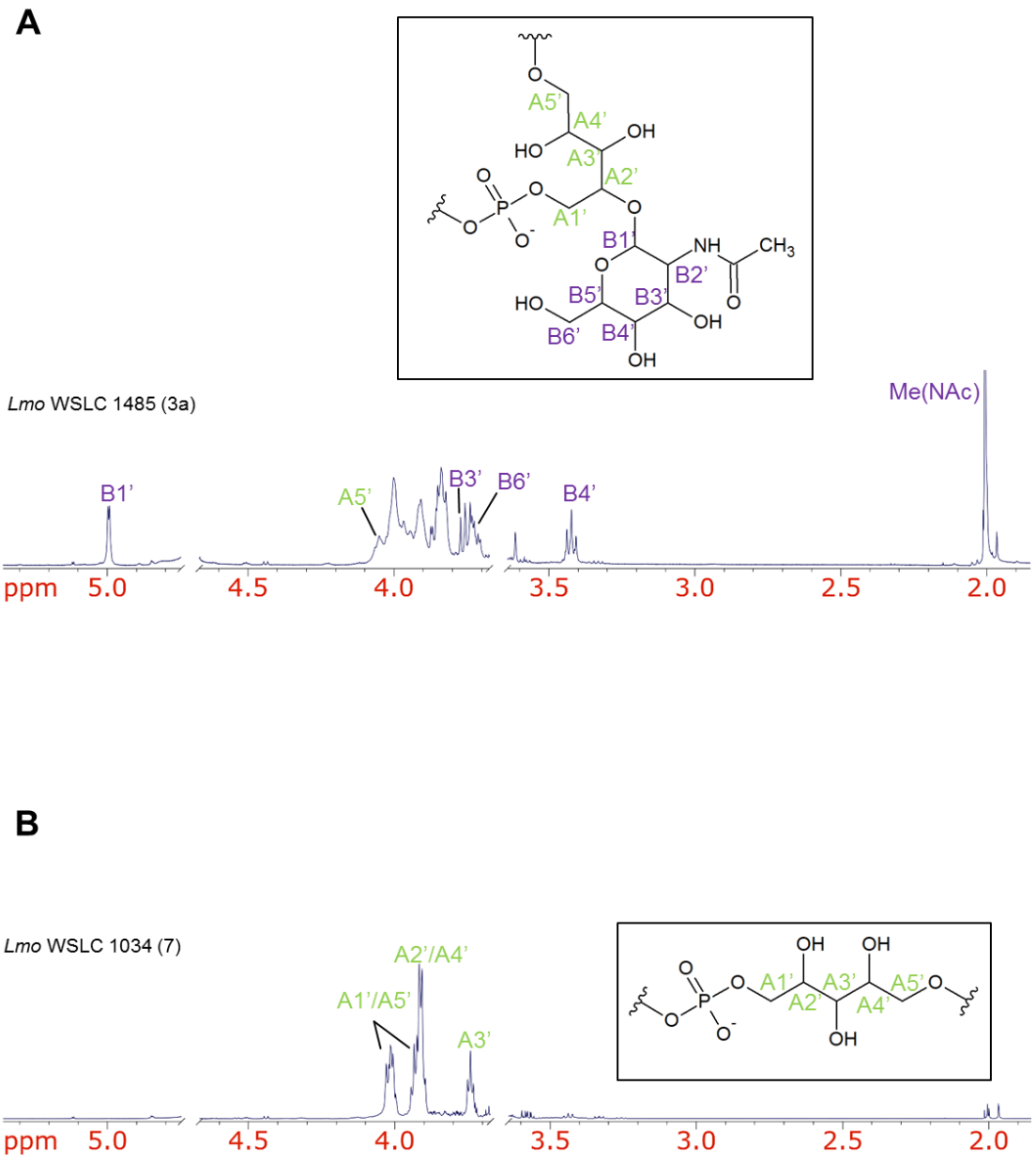

Figure S2. ^{1}H NMR spectra of WTA polymers from *Lmo* WSLC 1485 (top) and *Lmo* WSLC 1034 (bottom). No anomeric signal is present for WSLC 1034. DQF-COSY, ^{1}H-^{13}C HSQC, ^{1}H-^{13}C HMBC and ^{1}H-^{31}P COSY spectra were used for resonance assignment of the WTA repeating units (inset).

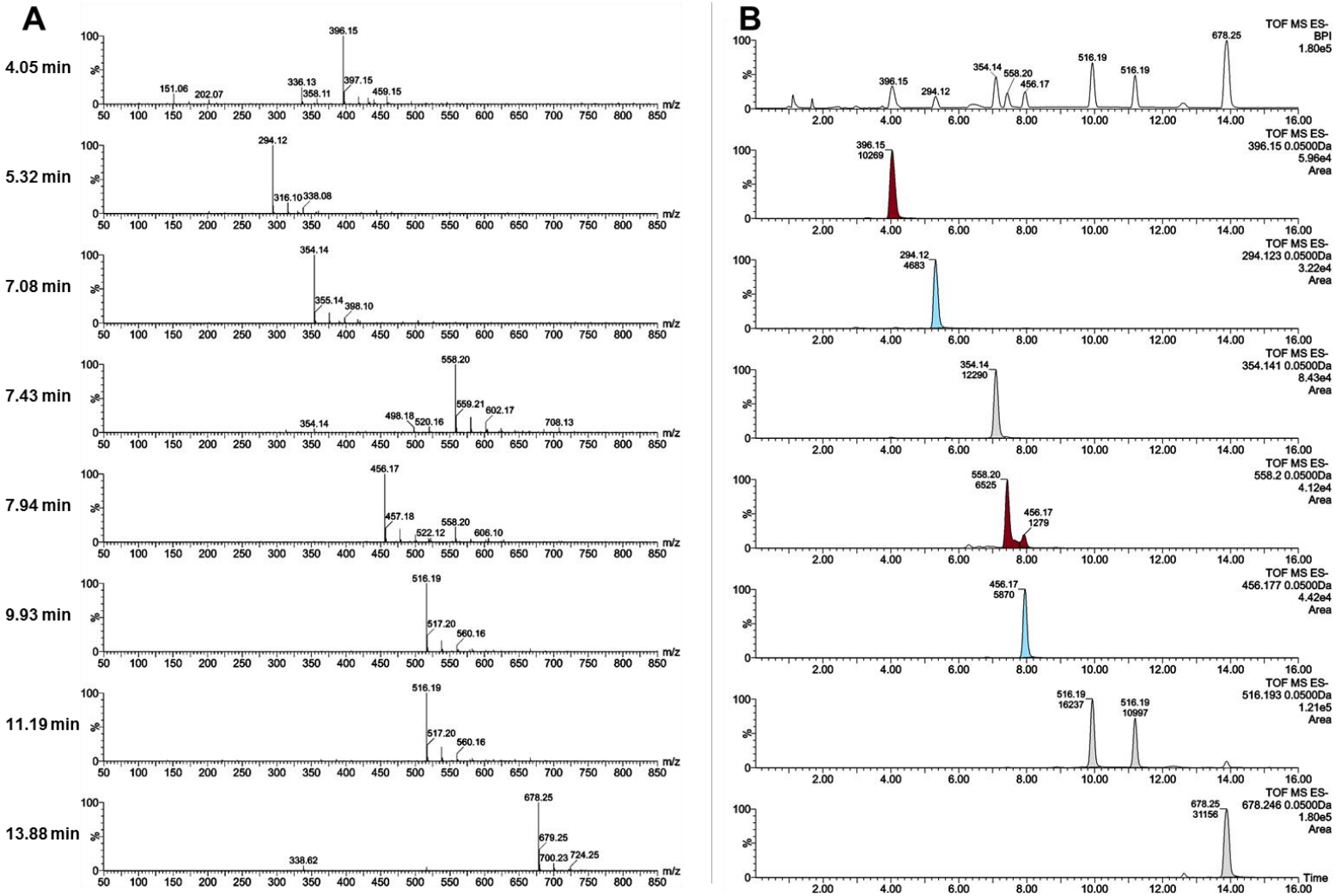

Figure S3. UPLC-MS data of depolymerized *Lmo* WSLC 1042 WTA. (A) All ESI-MS spectra of the relevant species (signals beneath peaks of UPLC-MS with indicated retention time). (B) Base peak ion chromatogram (BPI; top) and extracted-ion chromatograms of selected *m/z* for integration to calculate the relative degree of *O*-acetylation (peaks labeled with *m*/*z* and area [arbitrary units]).

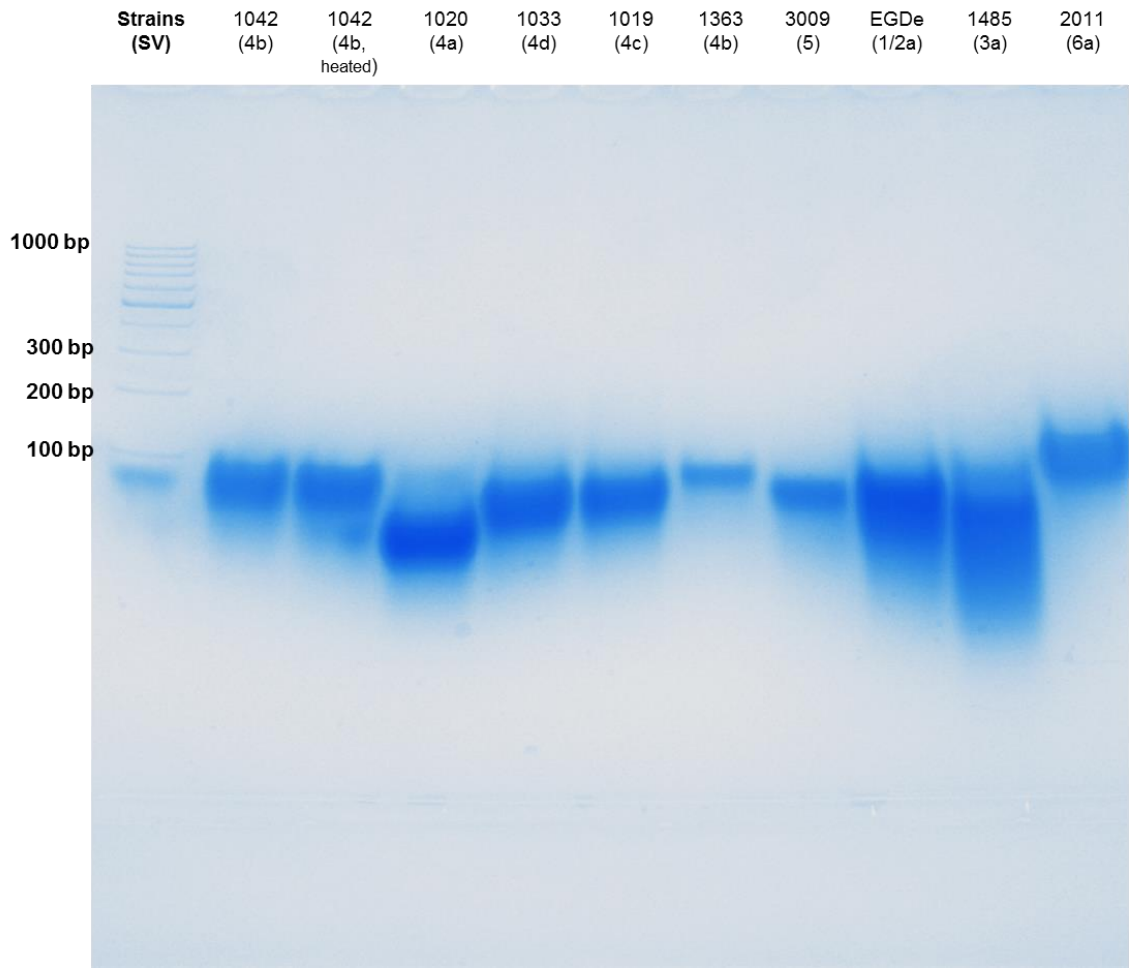

Figure S4. Native PAGE analysis of purified WTA polymers. 5 µg of purified WTA polymer from each strain that represents different serovars were loaded. The one hundred bp DNA ladder (the very left lane) was used as a control.

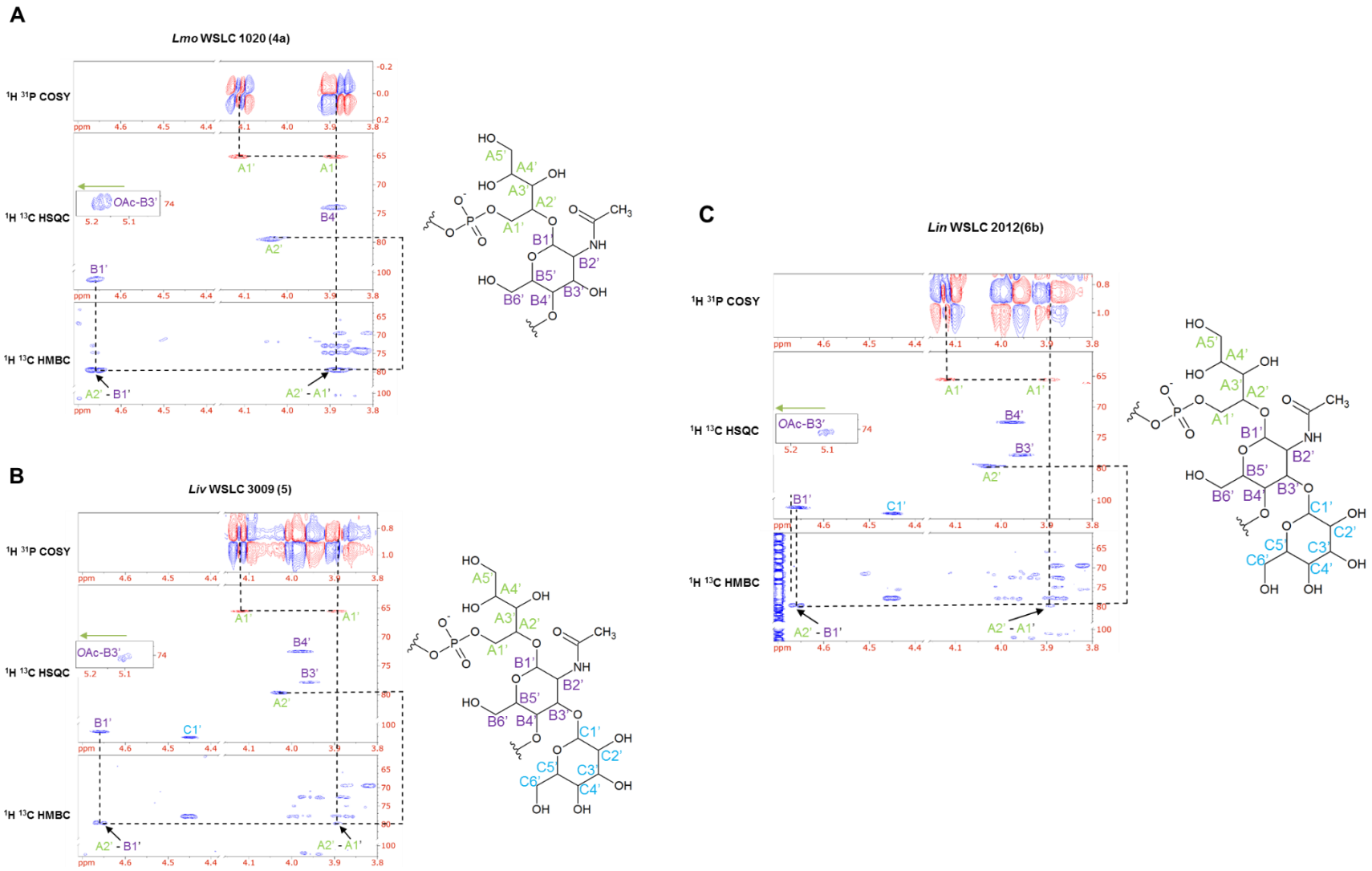

Figure S5. Details of ^{1}H-^{13}C HSQC, ^{1}H-^{13}C HMBC and ^{1}H-^{31}P COSY spectra of *Lmo* WSLC 1020 (A) and *Liv* WSLC 3009 (B), and *Lin* WSLC 2012 (C). Residue A: Rbo. B: GlcNAc. C: Glc.

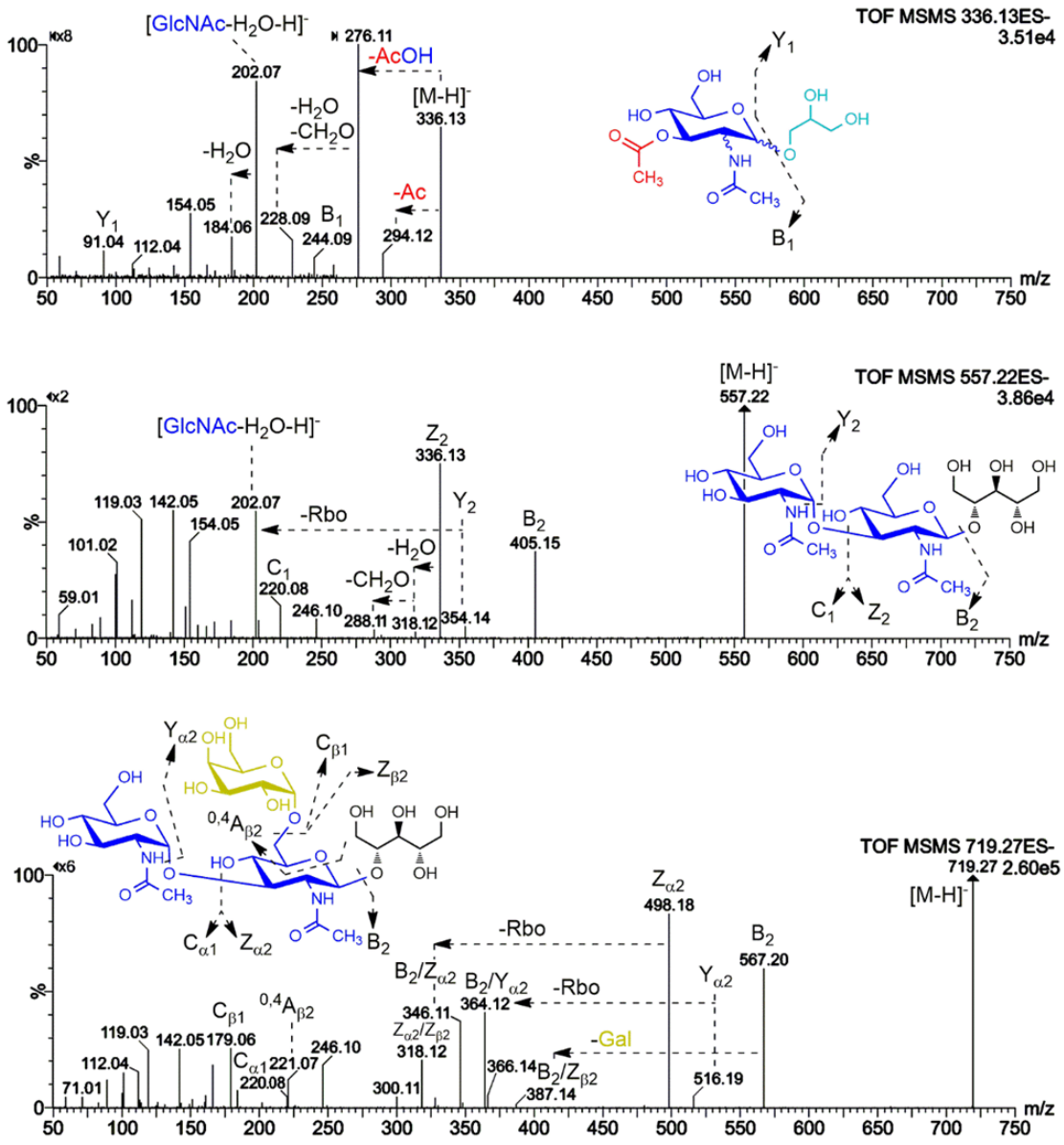

Figure S6. Structural elucidation of *m/z* 336, *m/z* 557, and *m/z* 719 from *Lin* WSLC 2011 (6a) by negative mode ESI-MS/MS.

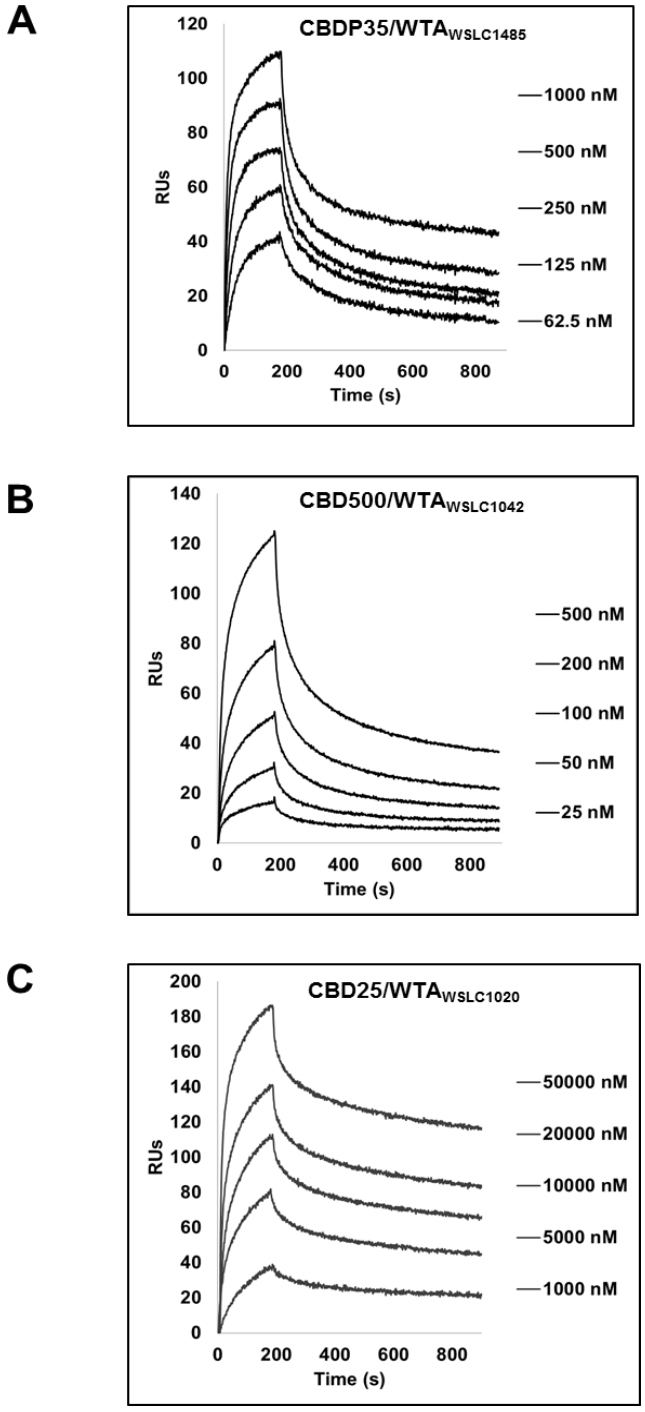

Figure S7. Kinetics of the interaction of CBDs with WTA polymers in a dose-response manner. The baseline response obtained with no (the 0 nM control) WTA analyte has been subtracted from the binding curves and is not shown. A series of WTA concentrations, shown in the legend, were used to study the binding to immobilized CBDP35 (A), CBD500 (B) and CBD025 (C), respectively. RU, relative units.